# Mechanism of Orlistat Hydrolysis by the Thioesterase of Human Fatty Acid Synthase

Valerie E. Fako,[†] Jian-Ting Zhang,[†,‡] and Jing-Yuan Liu*,[†,§]

[†]Department of Pharmacology and Toxicology and [‡]IU Simon Cancer Center, Indiana University School of Medicine, 980 West Walnut Street, Indianapolis, Indiana 46202, United States

[§]Department of Computer and Information Science, Indiana University-Purdue University, 635 Barnhill Drive, Indianapolis, Indiana 46202, United States

**S** Supporting Information

**ABSTRACT:** Fatty acid synthase (FASN), the sole protein capable of de novo synthesis of free fatty acids, is overexpressed in a wide variety of human cancers and is associated with poor prognosis and aggressiveness of these cancers. Orlistat, an FDA-approved drug for obesity treatment that inhibits pancreatic lipases in the GI tract, also inhibits the thioesterase (TE) of human FASN. The cocrystal structure of TE with orlistat shows a pseudo TE dimer containing two different forms of orlistat in the active site, an intermediate that is covalently bound to a serine residue (Ser$^{2308}$) and a hydrolyzed and inactivated product. In this study, we

attempted to understand the mechanism of TE-catalyzed orlistat hydrolysis by examining the role of the hexyl tail of the covalently bound orlistat in water activation for hydrolysis using molecular dynamics simulations. We found that the hexyl tail of the covalently bound orlistat undergoes a conformational transition, which is accompanied by destabilization of a hydrogen bond between a hydroxyl moiety of orlistat and the catalytic His$^{2481}$ of TE that in turn leads to an increased hydrogen bonding between water molecules and His$^{2481}$ and increased chance for water activation to hydrolyze the covalent bond between orlistat and Ser$^{2308}$. Thus, the conformation of the hexyl tail of orlistat plays an important role in orlistat hydrolysis. Strategies that stabilize the hexyl tail may lead to the design of more potent irreversible inhibitors that target FASN and block TE activity with greater endurance.

**KEYWORDS:** thioesterase, fatty acid synthase, orlistat
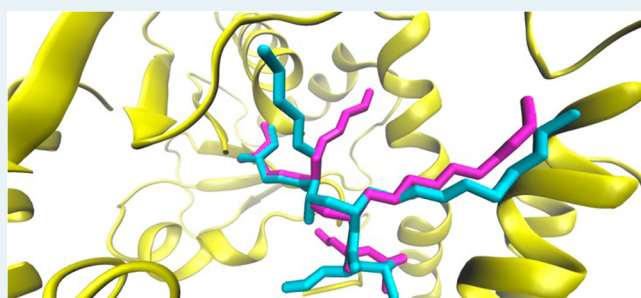
## ■ INTRODUCTION

Fatty acid synthase (FASN) is the sole protein capable of de novo synthesis of free fatty acids, most commonly 16-carbon palmitate.[1] Human FASN is overexpressed in a wide variety of human cancers, and this overexpression correlates with higher metastatic potential and poor prognosis.[2] FASN overexpression is also associated with increased resistance to cancer chemo-therapeutics in breast and pancreatic cancer cells,[3] indicating that FASN is an attractive target for chemosensitization.

Human FASN consists of seven reaction domains: β-ketoacyl synthase (KS), malonyl/acetyltransferase (MAT), β-hydrox-yacyl dehydrase (DH), enoyl reductase (ER), β-ketoacyl reductase (KR), acyl carrier protein (ACP), and thioesterase (TE).[4] De novo synthesis of fatty acids by FASN begins with condensation of acetyl-CoA and malonyl-CoA, and continues with elongation of the fatty acid chain, which is tethered to the phosphopantetheine cofactor of ACP, via a repeating cycle that adds two carbons each cycle.[5] At the end of elongation, TE cleaves the thioester bond between the fatty acid chain and the phosphopantetheine of ACP and releases the free fatty acid.[6]

The TE domain of FASN is a member of the serine hydrolase family, with the canonical Ser−His−Asp catalytic triad. The hydrolysis of the thioester bond between fatty acid and the phosphopantetheine of ACP involves the acceptance of a hydrogen atom from His$^{2481}$ by the sulfur atom of the phosphopantetheine and the transfer of fatty acid chain to Ser$^{2308}$, forming an acyl-enzyme intermediate. Then the catalytic nitrogen atom of His$^{2481}$ hydrogen bonds and activates a water molecule, which then undergoes nucleophilic attack of the carbonyl carbon of the acyl-enzyme intermediate, and releases the fatty acid from Ser$^{2308}$ and regenerates Ser$^{2308}$ and His$^{2481}$.[7] Active site inhibitors of FASN TE including orlistat can prevent the transfer of fatty acid from ACP to Ser$^{2308}$ of TE.

Orlistat (Figure 1A) is an FDA-approved drug for obesity treatment that inhibits pancreatic lipases in the gastrointestinal tract, but has also been shown to inhibit TE of FASN.[8] In addition, orlistat sensitizes FASN-mediated drug resistance in breast and pancreatic cancer cells;[3] induces endoplasmic reticulum stress,[9] apoptosis,[10] G1/S arrest in cancer cells;[11] and inhibits angiogenesis and proliferation of endothelial
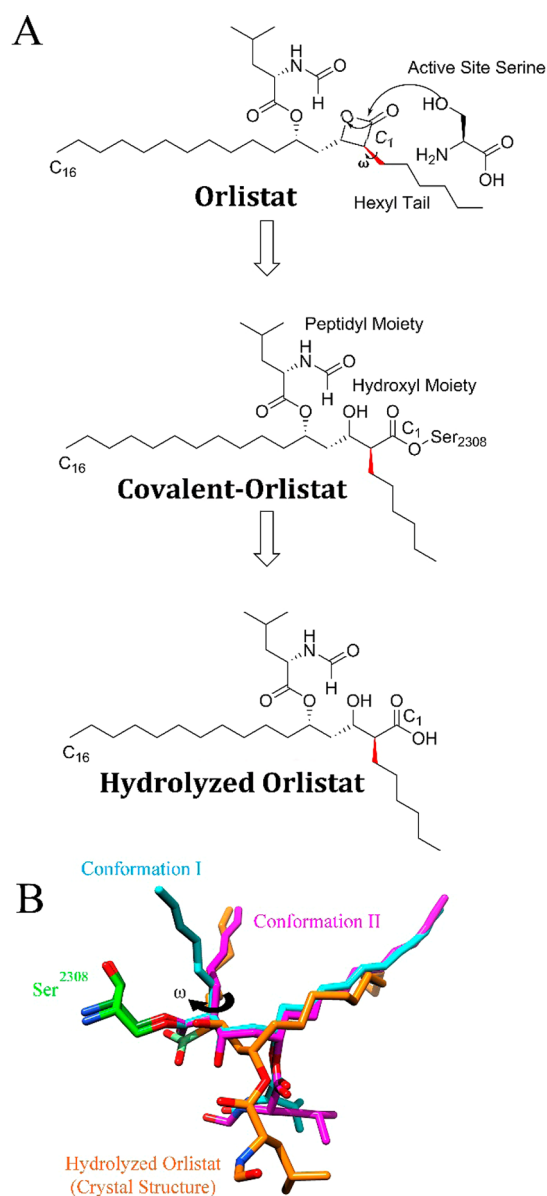
**Figure 1.** (A) Catalytic mechanism of orlistat hydrolysis by FASN TE. The active site Ser[2308] of TE nucleophilically attacks the $C^1$ carbon of the $\beta$-lactone moiety of orlistat to form a covalent bond between Ser[2308] and orlistat. Orlistat is then hydrolyzed and inactivated by TE. The $\omega$ dihedral angle of the hexyl tail that defines conformations I and II is depicted in red. (B) Alignment of average structures of covalent-orlistat in conformations I (cyan) and II (magenta) from the first simulation and the hydrolyzed orlistat from the crystal structure (orange). The Ser[2308] portion of covalent-orlistat is shown in green, and the hydrolyzed group in hydrolyzed orlistat is shown in light green.

cells,[12] possibly by inhibiting FASN. Computational docking analysis shows that orlistat binds to the ligand binding site in TE,[13] and the cocrystal structure of human FASN TE with orlistat (ID: 2PX6) shows that orlistat is indeed present in the active site of TE.[14] Interestingly, in the same cocrystal structure, orlistat exists both as a hydrolyzed product and as a covalently bound intermediate (covalent-orlistat), in which the C1 carbon of the $\beta$-lactone cyclic ester moiety of orlistat forms a covalent bond with the active site Ser[2308] (Figure 1A). In addition, the hexyl tail of orlistat appears to adopt two different

conformations in the covalent-orlistat and hydrolyzed product. It was speculated that the hexyl tail of covalent-orlistat may pack against His[2481] and prevent the access and activation of a water molecule needed for hydrolysis of the covalent bond between orlistat and Ser[2308].[14] However, whether the conformation transition of the hexyl tail occurs prior to the catalysis, and whether and how the transition contributes to catalysis is unknown.

In this study, we examined the potential role of the hexyl tail in water activation for orlistat hydrolysis using molecular dynamics (MD) simulations and found that the hexyl tail of covalent-orlistat shifts from one conformation to another within 35 ns simulations. However, the shift of the hexyl tail does not increase the accessibility of water molecules to the active site. Instead, this shift destabilizes a hydrogen bond between the catalytic nitrogen atom of His[2481] and the hydroxyl moiety of covalent-orlistat, allowing a water molecule to be activated via hydrogen bonding with His[2481] in a proper orientation for catalysis. Taken together, we conclude that the hexyl tail in covalent-orlistat can shift from one conformation to another, which plays an important role in orlistat hydrolysis by TE.

## ■ EXPERIMENTAL METHODS

**Orlistat Parameterization.** Covalent-orlistat is a non-natural residue, and therefore, parameters must be developed for Molecular Mechanics (MM) calculations. To achieve this goal, the coordinates of covalent-orlistat in TE were acquired from the Protein Data Bank (ID: 2PX6). The charges for covalent-orlistat are developed manually by a similar procedure described by Cornell et al.[15] Briefly, covalent-orlistat and Ser[2308], as well as the adjacent tyrosine residues (Tyr[2307] and Tyr[2309]) on either side of Ser[2308], were removed from the enzyme and capped by retaining the peptide backbone from Tyr[2307] and Tyr[2309], resulting in an N-terminal blocking cap that consists of a −(CO−CH$_3$) group and a C-terminal blocking cap that consists of a −(NH−CH$_3$) group (Supporting Information, Figure S1A). The model system was optimized at the B3LYP/6-31G* level of theory using the Quantum Mechanics (QM) package Gaussian03. Bond lengths and angles were optimized with dihedral angles between all heavy atoms kept frozen, to ensure that the charge development of orlistat reflects the charge distribution of the conformation seen in the crystal structure. The electrostatic potential of the ligand was then calculated with Gaussian03 using the HF/6-31G* level of quantum mechanical theory. Next, the atomic charges of the ligand were calculated in two steps by restrained electrostatic potential (RESP) charge fitting. In the first step, the charges of the caps, which sum to zero, were defined and the charges for the remainder of the atoms were calculated by RESP. In the second step, charges for all atoms were fixed except for methyl (−CH$_3$) and methylene (−CH$_2$) hydrogens. Charge calculations were repeated to ensure that rotationally degenerate atoms had equivalent charges. We intended to introduce as few new parameters as possible, and analogy to the existing ff03 atom types allowed us to define all missing values for covalent-orlistat (see Supporting Information, Figure S2A and Table S1 for more information). Using UCSF Chimera,[16] the caps were then removed, and the orlistat-Ser[2308] residue was reattached to the enzyme by aligning the newly optimized molecule with the original orlistat molecule, as seen previously by Pemble et al.[14]

**Validation of Covalent-Orlistat Parameterization.** To verify that the MM parameters developed for covalent-orlistat

agree with optimal geometries of the $\omega$ dihedral angle determined by QM, a rotational dihedral scan with angles differing by 10 degrees was performed by both ab initio QM and MM. The initial structure used for the dihedral angle scan was prepared as follows: Covalent-orlistat, previously optimized by Gaussian03 as mentioned above, and the two residues adjacent to orlistat were removed from the rest of the enzyme using Chimera. These tyrosine residues were modified to N-terminal and C-terminal glycine residues to create a 3-mer peptide containing covalent-orlistat (Supporting Information, Figure S1B). To avoid electrostatic interaction between the N-terminal amino group and the C-terminal carboxyl group, the torsion angles of this 3-mer peptide were adjusted into an extended conformation. The thirty-six rotamers of the $\omega$ dihedral angle were created using Chimera. The single point ab initio energy of each rotamer was calculated using Gaussian03 with the HF/6-31G* level of quantum mechanical theory. On the MM side, the potential energy surface of the 3-mer peptide was calculated using a nonperiodic vacuum model with the sander module of AMBER. Each rotamer was minimized using 500 steps of steepest descent minimization. To ensure that the conformation of each rotamer was not changed dramatically during minimization, all atoms were weakly restrained by 25 kcal/mol/$\text{Å}^2$ in Cartesian space using harmonic potential.

**Molecular Modeling and MD Simulation.** Missing loops in the crystal structure of TE were modeled using ModLoop.[17] Both the ff03 parameters and hydrogen atoms were assigned to the protein by the LeAP module of AMBER9. LeAP also added TIP3 water molecules to solvate the structure in a box with a distance of 8 Å between the wall and the closest atom in the system, in addition to appropriate counterions to neutralize the system. To calculate the long-range electrostatic interactions, Particle Mesh Ewald was used. The nonbonded cutoff was set to 8.0 Å. Prior to performing a production MD simulation, the system was equilibrated by a five-step protocol. First, the solvated system was minimized by 500 steps of steepest descent minimization followed by 500 steps of conjugate gradient minimization with all protein–ligand atoms in the system being restrained by 500 kcal/mol/$\text{Å}^2$ in Cartesian space using harmonic potential. Next, the energy of the whole system was minimized by removing the restraints in place and 10 000 steps of steepest descent minimization followed by 15 000 steps of conjugate gradient minimization. In the third step, the system was heated with a restraint of 10 kcal/mol/$\text{Å}^2$ to the protein from 0 to 300 K gradually over a duration of 50 ps controlled by Langevin dynamics with a collision frequency of 2 ps$^{-1}$. The system was then equilibrated by constant pressure dynamics simulation with a weak restraint of 10 kcal/mol/$\text{Å}^2$ to the protein with isotropic position scaling for 50 ps at 300 K. The reference pressure was set as 1 bar, with a pressure relaxation time of 1.0 ps. Finally, the system was further and fully equilibrated for additional 60 ps at 300 K using constant volume periodic boundaries, which was indicated by stable structure, energies, and temperatures. This step was controlled by Langevin dynamics with a collision frequency of 2 ps$^{-1}$ and a pressure relaxation time of 2 ps. The SHAKE procedure, which weakly constrains bonds involving hydrogen atoms, was applied to each step of the simulation. A total of 35 ns of production MD were simulated using the same conditions as the equilibration step. Two replicate simulations were performed using the same initial structure and the same conditions. An MD simulation with a truncated version of orlistat in which the hexyl tail was virtually changed to a methyl group (Supporting

Information, Figure S1C) was also performed using the same procedure described above. Additionally, the 3-mer peptide containing covalent-orlistat was solvated and a total of 100 ns of production MD were simulated using the above same procedure. To examine the effects of crystal packing on the behavior of covalent-orlistat, a simulation for FASN TE chains involving crystal contacts that may affect the covalent-orlistat binding mode was performed for 35 ns using the same procedure described above, but equilibrated for 5 ns due to the interchain movements.

**Free Energy Calculations.** To examine the free energy of the covalent-orlistat ligand in each hexyl tail conformation, a total of 50 snapshots over the course of each conformation in each simulation were extracted from the simulation trajectories of FASN TE. The free energy was calculated and decomposed to covalent-orlistat residue using the MM_PBSA module of AMBER by the equation $PB^{tot} = PB^{sol} + \text{gas}$, where $PB^{sol} = PB^{sur} + PB^{cal}$ and gas = ELE + VDW + INT. $PB^{sur}$ is described as the hydrophobic contributions to solvation free energy for PB calculations, and $PB^{cal}$ is described as the reaction field energy calculated by PB. ELE is the nonbonded electrostatic energy +1,4-electrostatic energy; VDW is the nonbonded van der Waals energy +1,4-van der Waals energy; and INT is the bond, angle, and dihedral energies. Additionally, to demonstrate that the two conformations of covalent-orlistat are independent, distinct, and not a result of the influence from the protein, two 100 ns trajectories were run for the 3-mer peptide, which is composed of covalent-orlistat bonded to Ser flanked by two Gly residues, and the free energy decomposed to covalent-orlistat was evaluated with a total of 50 snapshots in each conformation using the MM_PBSA module.

**Trajectory Analysis.** The conformational transition throughout the simulation was studied by analyzing the root-mean-square deviation (RMSD) of covalent-orlistat and the $\omega$ dihedral angle of the hexyl tail by ptraj. To monitor structural stability, RMSD, root-mean-square fluctuation (RMSF), and secondary structure analysis were calculated by the ptraj module of AMBER9. Water molecules in the active site of the enzyme were determined using VMD by searching for the water molecules within 3.5 Å of the catalytic nitrogen of His$^{2481}$ and within 4.0 Å of the carbonyl carbon of covalent-orlistat that the water molecule attacks. Hydrogen bonds between polar atoms (N, O, S, F) in the system were examined using VMD with the criteria of a donor–acceptor distance of 3.5 Å and an angle cutoff of 20 degrees. The donor–acceptor distance for strong hydrogen bonding required for catalysis between water molecules and His$^{2481}$ was set to 3.0 Å. Finally, all statistical calculations were performed using a two-tailed student's $t$ test with Prism5 (GraphPad).

## ■ RESULTS

**Covalent-Orlistat MM Parameter Verification by Quantum Mechanics.** Figure 1A shows the structures of free, covalent-, and hydrolyzed orlistat. The two conformations adopted by the hexyl tails in covalent- and hydrolyzed orlistat in TE in the crystal structure were assigned as conformations I and II (Figure 1B), respectively, which are defined by the $\omega$ angle of the hexyl tail (Figure 1A,B). The hexyl tail of the covalent-orlistat in conformation I has an $\omega$ angle of 337.97° and is accommodated in pocket I or "short-chain pocket" defined by residues Thr$^{2342}$, Tyr$^{2343}$, and Tyr$^{2462}$ of TE while the hexyl tail of hydrolyzed orlistat in conformation II has an $\omega$ angle of 139.54° and interacts with residues in pocket II or

"shift pocket" defined by residues Tyr[2309], Tyr[2343], and Ala[2430] as previously described.[14]

In order to examine the behavior of covalent-orlistat within the active site of TE prior to hydrolysis using an MD simulation approach, we first parametrized the Ser[2308] residue covalently bound to orlistat using the well-established procedure from the AMBER manual (see Experimental Methods and Supporting Information).[18] We next tested if our developed AMBER parameters could reproduce the ab initio energy profile for the $\omega$ dihedral angle of the hexyl tail that defines conformation I and II in the crystal structure by performing QM and MM dihedral angle scans of a 3-mer peptide containing covalent-orlistat attached to a Ser residue in the middle (Figure S1B). As shown in Figure S2B, the MM method using the AMBER parameters yielded an energy profile that is very similar to the curve generated by the ab initio method, with both profiles showing two minima and two maxima. The two maxima appeared at 8.2° and 248.2° in the ab initio curve and at 5.3° and 246.8° in the MM curve, indicating a good agreement. The two minima appeared at 158.2° and 308.2° in the ab initio curve and at 158.4° and 306.4° in the MM curve, which not only agree with each other very well but are similar to the $\omega$ angles (139.54° and 337.97°) of the hexyl tail of covalent- and hydrolyzed orlistat found in the crystal structure, respectively. Interestingly, the QM energy barrier separating the two hexyl tail conformations is 28.35 kcal/mol, which is considerably high. Thus, we conclude that covalent-orlistat was parametrized properly for MD simulations and that the hexyl tail of covalent-orlistat may adopt two distinct conformations, as observed in the crystal structure, before hydrolysis.

**Two Distinct Conformations of the Hexyl Tail in Covalent-Orlistat.** To show that the hexyl tail of covalent-orlistat can adopt both $\omega$ angle conformations observed in the crystal structure without the influences from TE, and that these conformations are energetically equivalent and independent conformations, we performed a 100 ns MD simulation of the 3-mer peptide containing covalent-orlistat (Supporting Information, Figure S1B). As shown in Supporting Information, Figure S2C, the $\omega$ dihedral angle begins at 303.79 ± 8.90° and changes to 178.53 ± 14.59° at 12.55 ns. It then flips back to 305.61 ± 9.68° at 52.09 ns. At 56.39 ns, the $\omega$ dihedral angle adopts 174.48 ± 15.44° again for the remainder of the simulation. The conformations of the hexyl tail of covalent-orlistat with these two major $\omega$ dihedral angles are similar to conformations I and II as observed in the cocrystal structure and, thus, covalent-orlistat without TE may adopt the same two conformations prior to hydrolysis. In addition, the calculated free energies of the 3-mer peptide containing covalent-orlistat in both conformations are nearly identical with an energy of −329.61 ± 7.55 kcal/mol in conformation I and −330.52 ± 7.81 kcal/mol in conformation II. Thus, we conclude that, without influence from the surrounding amino acid residues of TE, the hexyl tail of covalent-orlistat can adopt two distinct but energetically equivalent and interchangeable conformations that are similar to the conformations seen in the cocrystal structure.

**Compatibility of Covalent-Orlistat MM Parameters with AMBER Force Field.** To further determine whether the developed parameters of covalent-orlistat are compatible with the AMBER force field, we examined MM minimizations of the model system of TE in complex with covalent-orlistat in an explicit water environment. The developed parameters successfully minimized the initial structure with a convergence criterion of 1.0 kcal mol$^{-1}$ Å$^{-1}$. During the 60 ps equilibration

period of the simulation, the RSMD of the whole protein was stable and remained less than 1.5 Å. To confirm that the AMBER parameters of covalent-orlistat are suitable for MD simulation studies, we monitored various parameters during 35 ns MD simulations. Both the temperature and energy remained constant with little deviation during equilibration and production MD runs of all three simulations. The RMSD of the main chain atoms (RMSD$^{TE}$) is less than 2.0 Å during the entire simulation process (Figure 2A), which is consistently
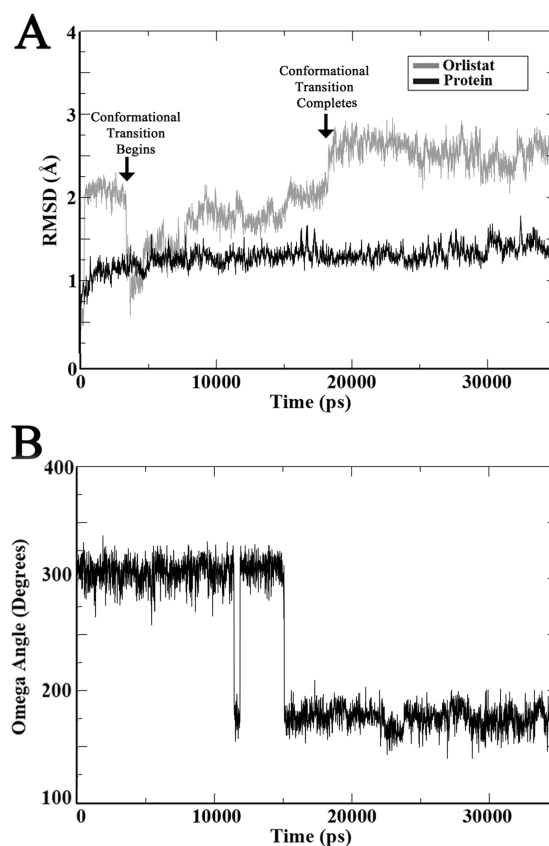


**Figure 2.** (A) RMSD of TE (black) and covalent-orlistat (gray) during the first simulation. Times when the conformational transition begins and completes are indicated. (B) $\omega$ dihedral angle of the hexyl tail of covalent-orlistat in the orlistat-TE complex along the simulation.

observed in all three simulations. These findings indicate that the overall protein structure is not disrupted or distorted throughout the simulations. The secondary structure of each residue is kept and agrees highly with the crystal structure. More importantly, the simulated B-factors of the protein (B-factor$^{TE}$) and covalent-orlistat (B-factor$^{orlistat}$) are comparable to the experimentally determined values[14] (Supporting Information, Figure S2D). Thus, we conclude that the parametrization is appropriate and compatible with the current AMBER force field.

**Conformational Transition of the Hexyl Tail in the FASN TE Domain.** The above studies showed that, in the absence of the TE protein, covalent-orlistat in the 3-mer peptide is able to adopt two different conformations for the hexyl tail, defined by the $\omega$ dihedral angle, that are independent and exchangeable. To determine if a conformational transition can also occur to the hexyl tail of covalent-orlistat in its binding pocket of the TE domain, and whether this transition has any effect on orlistat hydrolysis, we first examined the conformation

**Table 1. Time Span of Conformation I and II, B Factor, and Free Energy for All Three Simulations**

|  | conformation | first | second | third | crystal struct. |
|---|---|---|---|---|---|
| time span (ps)[a] | I | 0–3400 | 0–600 | 0–4000 | N/A |
|  | II | 18 250–35 000 | 4000–35 000 | 11 400–35 000 | N/A |
| B-factor[TE] |  | 43.8 ± 31.0[b] | 25.2 ± 19.4[b] | 38.64 ± 33.05[b] | 36.6 |
| B-factor[orlistat] |  | 77.1 | 69.2 | 83.4 | 60.2 |
| $G^{covalent-orlistat}$ (kcal/mol) | I | −130.29 ± 6.2[b] | −131.05 ± 6.92[b] | −131.60 ± 7.03[b] | N/A |
|  | II | −136.75 ± 5.47[b] | −139.05 ± 6.86[b] | −135.25 ± 7.19[b] | N/A |

[a]The time span in which the hexyl tail adopted each conformation in each simulation was determined by examining the RMSD of orlistat in conjunction with the $\omega$ angle transition. The time during which the transition was taking place was not included in our calculations. [b]Standard deviation.
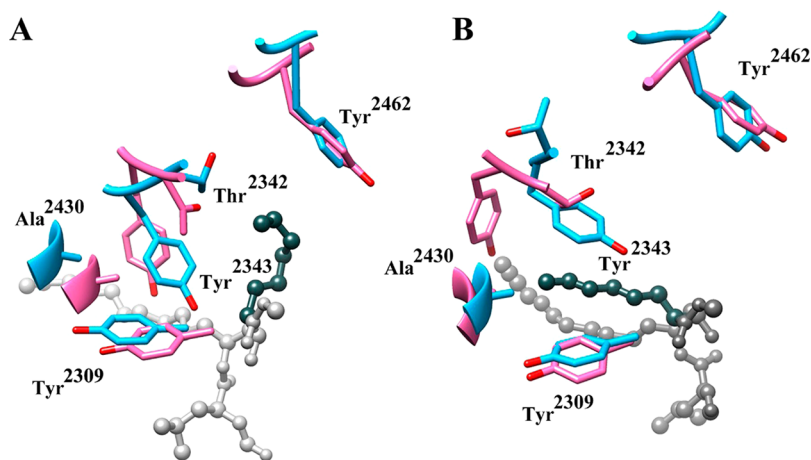


**Figure 3.** (A) Average structure (cyan) from the simulation when hexyl tail adopts conformation I is aligned with the crystal structure of covalent-orlistat (pink). (B) The average structure (cyan) from the simulation when hexyl tail adopts conformation II is aligned with the crystal structure of the hydrolyzed orlistat (pink). In both panels, orlistat, shown in gray with the hexyl tail in dark green, short-chain (Thr[2342], Tyr[2343] and Tyr[2462]), and shift pocket residues (Tyr[2309], Tyr[2343], Ala[2430]) are depicted.

of the hexyl tail during the three independent 35 ns simulations of the TE-covalent-orlistat complex.

The conformational transition of the hexyl tail can be examined by two criteria: the RMSD and the $\omega$ dihedral angle of the covalent-orlistat. We first examined the RMSD value of covalent-orlistat throughout each simulation and observed that the hexyl tail remained in one conformation, as noted by a stable RMSD, during the initial 3400 ps of the simulation until transitioning to a second conformation, which was completed at 18 250 ps when the RMSD of covalent-orlistat regained stability (Figure 2A). Similar conformational transitions but at different times were also observed in two other independent simulations with time spans of each conformation shown in Table 1 and Figure S3A, B. In the Supporting Information, Supplemental Video S1 shows a representative simulation of the conformational transition of the hexyl tail.

We next determined if the two conformations observed in these simulations are equivalent to and possibly represent conformations I and II observed in the crystal structure, by examining the $\omega$ dihedral angles throughout each simulation. We found that there is a clear change in the $\omega$ angle between the two stable states of covalent-orlistat (Figure 2B, Supporting Information, S3A, B). In the three simulations, the average $\omega$ angles ranges from 304.89 to 309.73° in stable state I and 172.68° to 176.32° in stable state II. Strikingly, the average $\omega$ angles in stable state I and II is respectively similar to the $\omega$ angles in conformation I (308.2°) and II (158.2°) determined by the ab initio method (Supporting Information, Figure S2B). Furthermore, the average $\omega$ angles are also similar to the $\omega$

angles of the two conformations in the crystal structure. These observations demonstrate that the two stable states of covalent-orlistat seen in the simulations indeed correspond to conformation I and II determined by ab initio method and crystal structure. It is noteworthy that there is a brief reversion of the $\omega$ angle from conformation II back to I and then a second $\omega$ angle transition to conformation II (at ~11 440–11 870 ps) was observed (Figure 2B). This is consistent with the $\omega$ dihedral angle transition noted with the 3-mer peptide.

Next, the free energy of the covalent-orlistat within TE in conformations I and II was calculated. Their free energies are nearly equivalent, ranging from −131.60 ± 7.03 to −130.29 ± 6.21 kcal/mol in conformation I and −139.05 ± 6.26 to −135.25 ± 7.19 kcal/mol in conformation II (Table 1), indicating that conformation II is unlikely a simple relaxation of conformation I. Together, these data show that the hexyl tail of covalent-orlistat in TE has shifted from conformation I to II during our simulations, which may resemble the conformational transition during catalysis as suggested by the crystal structure.

**Interactions of the Hexyl Tail with the Binding Pockets.** As discussed above, there are two pockets of residues in the crystal structure that accommodate the hexyl tail of covalent-orlistat in conformation I and hydrolyzed orlistat in conformation II and they are called short-chain pocket and shift pocket, respectively.[14] The short-chain pocket (or pocket I as we refer to) consists of residues Thr[2342], Tyr[2343], and Tyr[2462], and the shift pocket (or pocket II) consists of residues Tyr[2309], Tyr[2343], and Ala[2430]. To examine how the hexyl tail of covalent-orlistat interacts with each set of residues during our

simulations, the average structure of the protein with covalent-orlistat in conformation I and II from a representative simulation was aligned with the crystal structures of covalent-orlistat and hydrolyzed orlistat, respectively. As shown in Figure 3A, the hexyl tail in conformation I clearly interacts intensively with the pocket I residues, but not as much with pocket II residues. In addition, pocket I residues in the simulated average structure adopt similar conformations to the crystal structure. However, the similarity of pocket II residues between the simulated and crystal structures is not as high (Figure 3B). Although Tyr$^{2309}$ and Ala$^{2430}$ can be aligned very well, it appears that Tyr$^{2343}$ adopts very different conformation from the crystal structure. In the crystal structure, Tyr$^{2343}$ packs against the hexyl tail of covalent-orlistat in conformation I, but it then undergoes conformation transition and does not pack against the hexyl tail of the hydrolyzed orlistat in conformation II. This observation raised the possibility that the conformational change of Tyr$^{2343}$ may promote shifting of the hexyl tail. In the simulations, however, the positioning of Tyr$^{2343}$ changes very little before and after the hexyl tail shifts and it continues to pack against the hexyl tail of covalent-orlistat in conformation II. This difference in the conformation of Tyr$^{2343}$ may be a result of the hydrolysis because we are comparing the covalent-orlistat in the simulated average structure with the hydrolyzed orlistat in the crystal structure. This finding suggests that the conformation transition of Tyr$^{2343}$ may happen after the conformation transition of the hexyl tail, and instead of promoting conformation transition of the hexyl tail, it may facilitate the release of the hydrolyzed orlistat.

**Crystal Packing Favors the Hexyl Tail in Conformation I.** To understand whether crystal contacts have any effects on the conformation of the hexyl tail, multiple FASN TE chains were created by crystal symmetry operation and were used to perform another 35 ns MD simulation. Due to the crowdedness effect of the crystal lattice, residues Arg$^{2352}$, Thr$^{2356}$, Pro$^{2357}$, Gly$^{2358}$, Cys$^{2359}$, Glu$^{2360}$, and Ala$^{2361}$ in a different chain (chain B) directly interact with the covalent-orlistat in the current chain (chain A). In addition, residues Tyr$^{2347}$ and Thr$^{2348}$ in chain B may indirectly affect hexyl tail conformation via interacting with pocket I residues of chain A. RMSD and $\omega$ angle of the covalent-orlistat in both subunits were examined. Unlike our previous simulations containing only one FASN TE chain, the hexyl tail of the covalent-orlistat molecule in chain A was constrained in conformation I as indicated by the $\omega$ angle (Figure 4A) and the low and stable RMSD (Figure 4B) throughout the simulation. Interestingly, when examining the covalent-orlistat molecules in chain B, the molecules behave similarly to the covalent-orlistat molecules from our FASN TE monomer simulations (Supporting Information, Figure S4).

**Catalytically Critical Interactions at the Active Site.** We first tested whether the shift of the hexyl tail may provide access of water molecules to the TE active site proposed by Pemble et al.[14] by searching for water molecules that are ≤3.5 Å to the catalytic nitrogen of histidine and ≤4.0 Å to the carbonyl carbon atom of the covalent bond between orlistat and serine.[19] Under this stringent condition, it appears that in both conformations, the active site can be occupied by a water molecule for a significant amount of the time (Table 2). We next determined whether the conformational transition affects the catalytically important salt bridge between Asp$^{2338}$ and His$^{2481}$ [7b] (Figure 5A). The constant occupancy of this salt bridge suggests that Asp$^{2338}$ and His$^{2481}$ couple tightly both
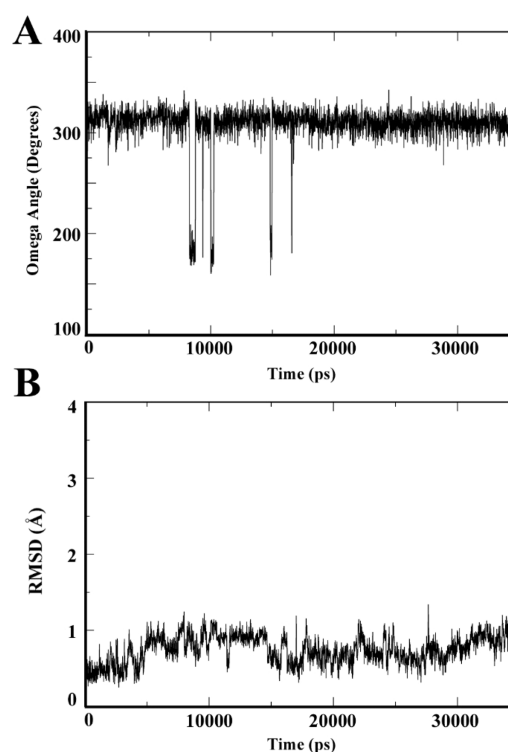


**Figure 4.** (A) $\omega$ angle of the hexyl tail in chain A during the simulation involving crystal contacts. (B) RMSD of the covalent-orlistat in chain A during the simulation involving crystal contacts.

before and after conformational transition of the hexyl tail, and its stability is not affected by the conformational transition (Figure 5B top panel, Table 2).

In addition to the salt bridge, we identified a hydrogen bond between the catalytic nitrogen of His$^{2481}$ and the hydroxyl moiety of covalent-orlistat (Figure 5A). In contrast to the occupancy of the Asp$^{2338}$-His$^{2481}$ salt bridge, the average occupancy of this hydrogen bond over all three simulations dropped significantly from 55.8% in conformation I to 19.3% in conformation II (Table 2, Figure 5B bottom panel). This agrees with the increased distance between the catalytic nitrogen of His$^{2481}$ and the oxygen of the hydroxyl moiety of covalent-orlistat when the hexyl tail adopts conformation II (Figure 5C, Table 2). A similar increase in this distance was also observed for the second and third simulations (Table 2). These results indicate that in each simulation, the potential for orlistat and His$^{2481}$ to form a hydrogen bond is diminished following the conformational transition. Therefore, the conformational transition of the hexyl tail does not appear to affect the salt bridge but destabilizes the hydrogen bond between the catalytic nitrogen of His$^{2481}$ and the hydroxyl moiety of covalent-orlistat.

**Activation of Catalytic Water Molecules.** To further understand how the conformational change of the hexyl tail affects catalysis, we next investigated the presence of potentially activated water molecules in the active site of TE with orlistat in both conformations using the following criteria. A catalytically active water molecule (a) must strongly hydrogen bond with His$^{2481}$ (at a distance ≤3.0 Å); (b) must be ≤4.0 Å from the carbonyl carbon atom of covalent-orlistat for nucleophilic attack; and (c) must form an optimal catalytic orientation angle of 105° ± 5° with the carbonyl carbon and the carbonyl oxygen (Figure 6A).[20] The average occupancy of water molecules that meet all the three criteria is significantly increased from 0.1% in

**Table 2. Catalytically Important Interactions at the Active Site**

| | conformations | first simulation | second simulation | third simulation |
|---|---|---|---|---|
| active site water occupancy (%) | I | 10.6 | 41.6 | 11.5 |
| | II | 31.4 | 28.9 | 31.5 |
| occupancy of Asp$^{2338}$-His$^{2481}$ salt bridge (%) | I | 100 | 98.4 | 100 |
| | II | 82.2 | 99.6 | 99.9 |
| occupancy orlistat-His$^{2481}$ H-bond (%) | I | 55.6 | 63.3 | 48.5 |
| | II | 6.0 | 25.9 | 25.9 |
| orlistat-His$^{2481}$ H-bond distance (Å) | I | 2.91 ± 0.21$^a$ | 2.83 ± 0.13$^a$ | 2.90 ± 0.18$^a$ |
| | II | 4.63 ± 0.99$^a$ | 3.51 ± 0.65$^a$ | 3.53 ± 0.70$^a$ |
| occupancy of H$_2$O-His$^{2481}$ H-bond (%) | I | 14.1 | 8.3 | 17.0 |
| | II | 57.8 | 36.9 | 25.6 |
| occupancy of activated H$_2$O molecule (%) | I | 0.3 | 0.0 | 0.0 |
| | II | 5.7 | 4.1 | 4.1 |

$^a$Standard deviation.
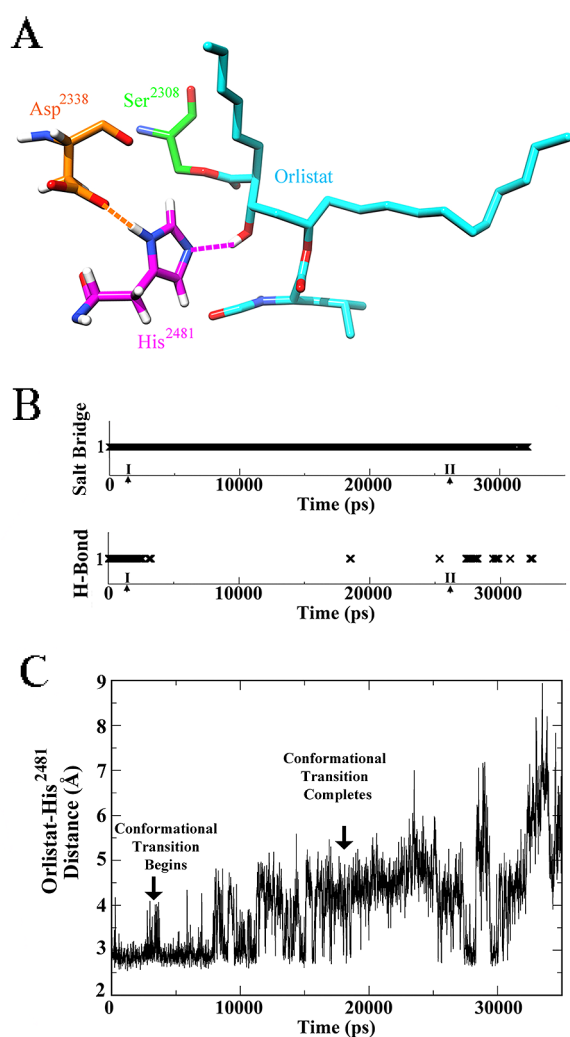


**Figure 5.** (A) Frame from the simulation showing the hydrogen bond between His$^{2481}$ and covalent-orlistat (magenta dashed line) and the salt bridge between His$^{2481}$ and Asp$^{2338}$ (orange dashed line) when covalent-orlistat adopts conformation I. Ser$^{2308}$, Asp$^{2338}$, and His$^{2481}$ residues of TE are depicted in green, orange, and magenta, respectively. (B) Occupancies of the salt bridge between Asp$^{2338}$ and His$^{2481}$ (upper) and hydrogen bond between His$^{2481}$ and hydroxyl group of orlistat (lower) are shown along the simulation. (C) The distance between the catalytic nitrogen atom of His$^{2481}$ and the oxygen atom of the hydroxyl group of covalent-orlistat along the simulation.
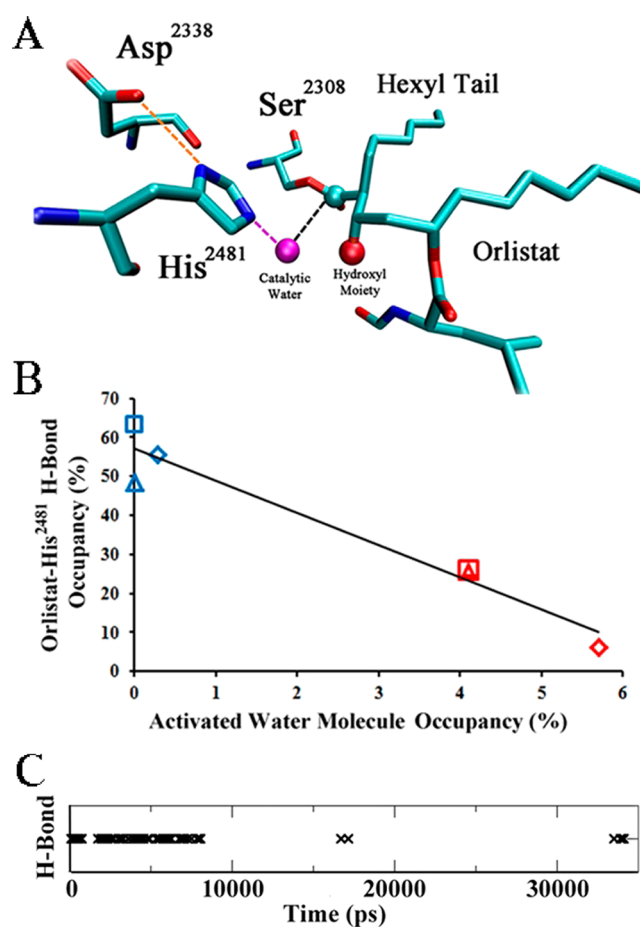


**Figure 6.** (A) Frame from the simulation showing an activated water molecule in the active site. Hydrogen bonds are depicted by dashed lines. C1 atom is highlighted by blue ball. (B) Correlation between the occupancy of the orlistat-His$^{2481}$ hydrogen bond and the occupancy of activated water molecules in conformations I (blue points) and II (red points) of the first (◇), second (□), and third (△) simulation. (C) The occupancy of the hydrogen bond between the truncated covalent-orlistat and His$^{2481}$ throughout the simulation.

conformation I to 4.6% in conformation II (Table 2). This observation suggests that when the hexyl tail is in conformation I, a water molecule is unlikely to be catalytically activated and the possibility of catalytic activation is significantly increased after the hexyl tail transitions to conformation II.

**Correlation of Interactions in the Active Site.** To understand how the conformational transition may affect the chance of activation of a water molecule for catalysis, we analyzed the ability of water molecules to form strong hydrogen bonds ($\leq 3.0$ Å) with the catalytic nitrogen of His[2481] before and after the conformational transition of the hexyl tail. As shown in Table 2, the occupancy of water molecules that can strongly hydrogen bond with His[2481] is increased from an average of 11% in conformation I to 40% in conformation II ($p = 0.051$).

Considering that there is a decrease in hydrogen bonding between His[2481] and the hydroxyl moiety of covalent-orlistat and an increase in hydrogen bonding between His[2481] and water molecules, it is possible that these two events are correlated. To test this possibility, we first calculated the occupancy of the hydrogen bond between His[2481] and covalent-orlistat when there is a water molecule in the active site that satisfies all catalytic criteria, which was 0.7%, 0.8% and 1.0% in the first, second and third simulation, respectively. We then performed a correlation analysis of the occupancy of the hydrogen bond between His[2481] and covalent-orlistat and the occupancy of activated water molecules that satisfy all criteria for a catalytic interaction in both conformations I and II. As shown in Figure 6B, there is a clear trend of linear correlation between these occupancies with a correlation coefficient of 0.94, indicating that a water molecule is more likely to catalytically interact with orlistat in the absence of the hydrogen bond between covalent-orlistat and His[2481]. Together, the above findings suggest that the hydrogen bond between covalent-orlistat and His[2481] may need to be abrogated to successfully activate a catalytic water molecule.

**Simulation of Truncated Orlistat Lacking the Hexyl Tail.** The above findings suggest that conformation I of the hexyl tail may help stabilize the hydrogen bond between His[2481] and covalent-orlistat. To test this possibility, we performed an MD simulation analysis using a truncated covalent-orlistat lacking the hexyl tail (Supporting Information, Figure S1C). For this purpose, the hexyl tail of covalent-orlistat in the crystal structure was virtually removed, parametrized, and simulated similarly as described above for the intact orlistat. Figure 6C shows that the hydrogen bond between His[2481] and the hydroxyl group of truncated covalent-orlistat was spontaneously and quickly disrupted at 8,190 ps. It remained in a disrupted state and did not reform for any significant amount of time during the remainder of the simulation. Interestingly, the occupancy of water molecules that can be potentially activated before and after disruption of the hydrogen bond is 0.9% and 4.3%, respectively, which is consistent with the observations of intact covalent-orlistat. Taken together with the results for intact covalent-orlistat, we conclude that the hexyl tail in conformation I likely stabilizes the hydrogen bond between His[2481] and covalent-orlistat, which prevents His[2481] from hydrogen bonding with and properly orienting and activating a water molecule for catalysis in the active site.

## ■ DISCUSSION

The serine hydrolases are one of the largest classes of enzymes and their catalytic mechanism has been studied since the 1960s.[21] The action of the canonical Ser−His−Asp catalytic triad has been extensively studied by experiments such as mutagenesis combined with enzymatic assays,[22] X-ray crystallography,[22,23] and NMR,[24] as well as by QM/MM computations.[25] The cleavage of the substrate involves two major steps.

First, the proton of the catalytic serine is abstracted by the histidine. The O$\gamma$ of Ser nucleophilically attacks the carbonyl carbon of the substrate to be hydrolyzed, forming a tetrahedral oxyanion intermediate. This intermediate collapses shortly and an acylenzyme is formed, which completes the acylation step of the reaction. In the second step, a water molecule is activated by deprotonation by the histidine, similar to the serine in the acylation reaction. The activated water molecule attacks the central carbonyl atom of the acylenzyme ester bond and forms an anionic tetrahedral intermediate again. Similarly, this intermediate collapses and results in the release of a carboxylic acid and regeneration of the active site.

FASN TE shares the canonical catalytic triad with other serine hydrolases.[26] The hydrogen bond network at the catalytic site is well-suited for the above catalytic mechanism and is also similar to other serine hydrolases.[26a,27] The special feature of the cocrystal structure of human FASN TE with orlistat (ID: 2PX6), however, is that orlistat is present in the active site of TE in two states: a state covalently bound to the enzyme indicating a reaction stopped at first step and a state of hydrolyzed product indicating a completed reaction. Interestingly, the hexyl tail of orlistat in these two different states adopts two different conformations (I and II). Whether the hexyl tail shifts before or after the reaction completion and whether and how the shift dominates the advancement to the second step of the catalysis is not clear.

In this study, we modeled covalent-orlistat in a 3-mer peptide and found that the two conformations in the crystal structure are stable conformations and energetically equivalent as determined using both QM and MM methods. This finding suggests that the covalent-orlistat can adopt both conformations prior to hydrolysis. In addition, the finding that the hexyl tail of covalent-orlistat in the 3-mer peptide can transit back and forth freely between conformations I and II shown by MM method further indicates that the conformational transition of the hexyl tail may play a critical role in the advancement of the catalysis to the second step. The fact that the two energetically equivalent conformations captured in the crystal structure are not equally reactive and the fact that the hexyl tail is not the site for the hydrolysis to happen suggest that the hexyl tail may exert its effects on the protein in large scale. Although combined quantum and molecular mechanical (QM/MM) method can predict activation barriers and stationary structural points for enzymatic reactions based on potential energy surfaces, it requires predefining up to only a few hundred QM atoms within a system.[28] This prerequisite limits the use of this method to solve the problem in this study. Because the conformational transition of the hexyl tail does not involve bond-breaking or -forming, the MM approach can be used to investigate the large scale effect of the hexyl tail on the enzyme. Our study shows that the hexyl tail in conformation I prevents the activation of a water molecule because of a hydrogen bond between the catalytic His[2481] and the hydroxyl moiety of orlistat. The conformation transition of the hexyl tail destabilizes this hydrogen bond and leads to formation of a hydrogen bond between His[2481] and water molecules, allowing the activation of a water molecule to hydrolyze the covalent bond between orlistat and Ser[2308]. Therefore, the conformation transition of the hexyl tail is critical and required for hydrolysis of covalent-orlistat. Here, we applied distance criteria and the Bürgi−Dunitz rule[20] in identifying an "activated" water molecule in the MM computational setting. Further studies using QM/MM methods once an "activated" water molecule is

identified by the MM method can investigate the bond breaking process and the complete reaction pathways, which may provide further support for the above findings by the MM methods.

Another interesting observation from the complex structure solved by Pemble et al. is the structure is that the result of cocrystallization of TE and orlistat, not from a crystal soaking experiment. During the lengthy cocrystallization process, protein and ligand are coincubated in solution and can freely react with each other without crystal packing restraints that are present in crystal soaking experiment.[14] Yet in this condition, only some of orlistat is hydrolyzed, suggesting that the nonhydrolyzed covalent-orlistat cannot be a result solely from crystal packing. Rather, the crystal lattice may selectively pack TE with covalent-orlistat in conformation I from solution in one asymmetric unit and TE with hydrolyzed orlistat in conformation II from solution in another asymmetric unit. Once crystals are formed, the covalent-orlistat in conformation I may not be able to transit to conformation II due to crystal lattice restraint and therefore remain in nonhydrolyzed state. Our simulation data agrees with the crystal structures and the above mechanism. In all our water-explicit simulations mimicking TE in solution without crystal contacts, the hexyl tail of covalent-orlistat undergoes a transition from conformation I to II indicated by its RSMD and the $\omega$ angle, whereas the subunit subjected to crystal packing is stabilized in conformation I.

We observed that the $\omega$ angles of covalent-orlistat in the 3-mer peptide can switch between conformation I and II freely. We also observed that the $\omega$ angles of hexyl tail in TE can switch between conformation I and II. However, most of the time, covalent-orlistat in TE adopts conformation II, raising the possibility that the binding of free TE in solution may stabilize conformation II. This agrees with the calculated free energies of covalent-orlistat in TE, which suggest conformation II is slightly more favorable. The slight preference to conformation II in free TE could be important for the conversion of orlistat, and it ensures sufficient time in conformation II for hydrolysis, which could be considerably quick compared with the conformation transition, to happen. This conclusion is supported by the fact that no covalent-orlistat in conformation II is captured in the cocrystal structure. On the other hand, crystal contacts may stabilize covalent-orlistat in conformation I as demonstrated by our simulation when crystal packing from another chain exists. This result further demonstrates that the two conformations of covalent-orlistat are equivalent and the final adopted conformation is susceptible to the surrounding environments from the protein. Taking both the experimental and computational observations into account, it is tempting to speculate that the conformational transition of the hexyl tail may be a rate-limiting step of orlistat hydrolysis.

We also showed that a hydrogen bond exists between the catalytic His[2481] residue and covalent-orlistat, which may inhibit orlistat hydrolysis. It appears that in conformation I, the strong interaction between the catalytic nitrogen atom of His[2481] and the hydroxyl moiety of covalent-orlistat greatly prevents water molecules from hydrogen bonding with the same atom of His[2481] and from adopting the proper orientation for activation and catalysis. When the hexyl tail transits from conformation I to II, the hydrogen bond between His[2481] and covalent-orlistat is disrupted, which frees and enables His[2481] to hydrogen bond with and activate water molecules to attack the carbonyl carbon of the orlistat-Ser[2308] residue. In the cocrystal structure, the

distance between the catalytic nitrogen atom of His[2481] and the hydroxyl moiety of covalent-orlistat is 3.9 Å in conformation I, representing a weak hydrogen bond between the two atoms. In agreement with our simulation, this distance increased to 5.4 Å in conformation II in the cocrystal structure. Although a distance of 3.9 Å in conformation I indicates a weak hydrogen bond, it should be considered that the crystal structure is a still snapshot of a protein in solid state, which may not capture the stronger hydrogen bonding event found in solution. Nevertheless, both the crystal structure and our simulation data suggest stronger interactions between the catalytic nitrogen atom of His[2481] and the oxygen atom of the hydroxyl group of covalent-orlistat in conformation I than in conformation II.

So we may conclude that the hexyl tail in conformation I favors a stronger interaction between the catalytic nitrogen atom of His[2481] and the oxygen atom of the hydroxyl group of covalent-orlistat, which prohibits hydrolysis. This is further validated by the simulation of TE covalently bound to a truncated orlistat lacking the long hexyl tail. The simulation shows that the hydrogen bond between His[2481] and the hydroxyl moiety of truncated covalent-orlistat is quickly and spontaneously disrupted, accompanied by an increase in activated water molecules in the active site for hydrolysis. Thus, the truncated orlistat may be more easily hydrolyzed than the intact orlistat. These results are intuitive in that truncated orlistat is structurally more closely related to the natural substrates of FASN TE. Interestingly, it has been found previously that ebelactone B, a $\beta$-lactone compound containing an ethyl group in the same position as the hexyl tail of orlistat, was more effective in inhibiting FASN TE activity than ebelactone A, which contains a methyl group,[8] leading to the speculation that this moiety may be important for stabilizing the covalent bound ligand in the TE active site and protecting it from hydrolysis.[29] Our data supports this hypothesis and provides a mechanistic model by demonstrating that the hexyl tail in conformation I is needed to stabilize the hydrogen bond that forms between His[2481] and the hydroxyl moiety of orlistat, which helps to prevent hydrolysis of the ligand. This stabilization is lost when the hexyl tail is removed, or undergoes conformation transition, likely leading to rapid hydrolysis shortly thereafter. Orlistat is a reversible inhibitor of FASN, although the conversion rate can be very slow. Considering that FASN overexpression may cause an increased metastatic potential, poorer prognosis, and resistance toward cancer chemotherapeutics in a wide variety of human cancers,[2,3] information from this study may help in the rational design of more potent irreversible TE inhibitors for anticancer treatment. By utilizing and stabilizing the hydrogen bond between the ligand and His[2481] and thereby inhibiting the activation of a water molecule for catalysis, it would be possible to design or discover inhibitors that covalently bond to TE and permanently disable its function. Another strategy for next generation compound design may be to use moieties that block the space in the active site near His[2481] that water molecules must occupy for activation. This may be achievable, as it has previously been shown in a similar case of inhibitors of *E. coli* TEM-1 $\beta$-lactamase. Although $\beta$-lactamases have a different catalytic triad from that of TE, they contain an active site Ser. Inhibitors of $\beta$-lactamase, such as penicillanic acid, inhibit the enzyme by acetylation of this active site Ser.[30] A modified form of penicillanic acid, 6$\alpha$-(hydroxymethyl) penicillanate, created by incorporating a hydroxymethyl moiety designed to displace the catalytic water molecule in the active site, resulted in a retarded

rate of hydrolysis of the acyl-enzyme intermediate.[31] The mechanism of action was later confirmed by X-ray crystallography.[31]

## ■ ASSOCIATED CONTENT

### Ⓢ Supporting Information

Extended simulation data and simulation video. This material is available free of charge via the Internet at http://pubs.acs.org.

## ■ AUTHOR INFORMATION

### Corresponding Author
*E-mail: jliu2@iupui.edu. Fax: (317) 274-1560. Tel.: (317) 274-7645.

### Notes
The authors declare no competing financial interest.

## ■ ACKNOWLEDGMENTS

## ■ REFERENCES

(1) Wakil, S. J. *Biochemistry* **1989**, *28*, 4523−4530.

(2) (a) Alo, P. L.; Visca, P.; Marci, A.; Mangoni, A.; Botti, C.; Di Tondo, U. *Cancer* **1996**, *77*, 474−482. (b) Epstein, J. I.; Carmichael, M.; Partin, A. W. *Urology* **1995**, *45*, 81−86. (c) Visca, P.; Sebastiani, V.; Botti, C.; Diodoro, M. G.; Lasagni, R. P.; Romagnoli, F.; Brenna, A.; De Joannon, B. C.; Donnorso, R. P.; Lombardi, G.; Alo, P. L. *Anticancer Res.* **2004**, *24*, 4169−4173. (d) Sebastiani, V.; Visca, P.; Botti, C.; Santeusanio, G.; Galati, G. M.; Piccini, V.; Capezzone de Joannon, B.; Di Tondo, U.; Alo, P. L. *Gynecol. Oncol.* **2004**, *92*, 101−105. (e) Takahiro, T.; Shinichi, K.; Toshimitsu, S. *Clin. Cancer Res.* **2003**, *9*, 2204−2212. (f) Innocenzi, D.; Alo, P. L.; Balzani, A.; Sebastiani, V.; Silipo, V.; La Torre, G.; Ricciardi, G.; Bosman, C.; Calvieri, S. *J. Cutaneous Pathol.* **2003**, *30*, 23−28. (g) Alo, P. L.; Amini, M.; Piro, F.; Pizzuti, L.; Sebastiani, V.; Botti, C.; Murari, R.; Zotti, G.; Di Tondo, U. *Anticancer Res.* **2007**, *27*, 2523−2527. (h) Liu, H.; Liu, J.-Y.; Wu, X.; Zhang, J. T. *Int. J. Biochem. Mol. Biol.* **2010**, *1*, 69−89.

(3) (a) Liu, H.; Liu, Y.; Zhang, J. T. *Mol. Cancer Ther.* **2008**, *7*, 263−270. (b) Yang, Y.; Liu, H.; Li, Z.; Zhao, Z.; Yip-Schneider, M.; Fan, Q.; Schmidt, C. M.; Chiorean, E. G.; Xie, J.; Cheng, L.; Chen, J. H.; Zhang, J. T. *Int. J. Biochem. Mol. Biol.* **2011**, *2*, 89−98.

(4) (a) Chirala, S. S.; Wakil, S. J. *Lipids* **2004**, *39*, 1045−1053. (b) Maier, T.; Jenni, S.; Ban, N. *Science* **2006**, *311*, 1258−1262.

(5) Smith, S. *FASEB J.* **1994**, *8*, 1248−1259.

(6) Joshi, A. K.; Witkowski, A.; Berman, H. A.; Zhang, L.; Smith, S. *Biochemistry* **2005**, *44*, 4100−4107.

(7) (a) Dodson, G.; Wlodawer, A. *Trends Biochem. Sci.* **1998**, *23*, 347−352. (b) Polgar, L. *Cell. Mol. Life Sci.* **2005**, *62*, 2161−2172.

(8) Kridel, S. J.; Axelrod, F.; Rozenkrantz, N.; Smith, J. W. *Cancer Res.* **2004**, *64*, 2070−2075.

(9) Little, J. L.; Wheeler, F. B.; Fels, D. R.; Koumenis, C.; Kridel, S. J. *Cancer Res.* **2007**, *67*, 1262−1269.

(10) (a) Carvalho, M. A.; Zecchin, K. G.; Seguin, F.; Bastos, D. C.; Agostini, M.; Rangel, A. L.; Veiga, S. S.; Raposo, H. F.; Oliveira, H. C.; Loda, M.; Coletta, R. D.; Graner, E. *Int. J. Cancer* **2008**, *123*, 2557−2565. (b) Dowling, S.; Cox, J.; Cenedella, R. J. *Lipids* **2009**, *44*, 489−498. (c) Knowles, L. M.; Yang, C.; Osterman, A.; Smith, J. W. *J. Biol. Chem.* **2008**, *283*, 31378−31384. (d) Samudio, I.; Harmancey, R.; Fiegl, M.; Kantarjian, H.; Konopleva, M.; Korchin, B.; Kaluarachchi, K.; Bornmann, W.; Duvvuri, S.; Taegtmeyer, H.; Andreeff, M. *J. Clin. Invest.* **2010**, *120*, 142−156. (e) Zecchin, K. G.; Rossato, F. A.; Raposo, H. F.; Melo, D. R.; Alberici, L. C.; Oliveira, H. C.; Castilho, R. F.;

Coletta, R. D.; Vercesi, A. E.; Graner, E. *Lab. Invest.* **2011**, *91*, 232−240.

(11) Knowles, L. M.; Axelrod, F.; Browne, C. D.; Smith, J. W. *J. Biol. Chem.* **2004**, *279*, 30540−30545.

(12) Browne, C. D.; Hindmarsh, E. J.; Smith, J. W. *FASEB J.* **2006**, *20*, 2027−2035.

(13) Cheng, F.; Wang, Q.; Chen, M.; Quiocho, F. A.; Ma, J. *Proteins* **2008**, *70*, 1228−1234.

(14) Pemble, C. W.; Johnson, L. C.; Kridel, S. J.; Lowther, W. T. *Nat. Struct Mol. Biol.* **2007**, *14*, 704−709.

(15) Cornell, W. D.; Cieplak, P.; Bayly, C. I.; Gould, I. R.; Merz, K. M.; Ferguson, D. M.; Spellmeyer, D. C.; Fox, T.; Caldwell, J. W.; Kollman, P. A. *J. Am. Chem. Soc.* **1995**, *117*, 5179−5197.

(16) Pettersen, E. F.; Goddard, T. D.; Huang, C. C.; Couch, G. S.; Greenblatt, D. M.; Meng, E. C.; Ferrin, T. E. *J. Comput. Chem.* **2004**, *25*, 1605−1612.

(17) Fiser, A.; Sali, A. *Bioinformatics* **2003**, *19*, 2500−2501.

(18) Cornell, W. D.; Cieplak, P.; Bayly, C. I.; Gould, I. R.; Merz, K. M.; Ferguson, D. M.; Spellmeyer, D. C.; Fox, T.; Caldwell, J. W.; Kollman, P. A. *J. Am. Chem. Soc.* **1995**, *117*, 5179−5197.

(19) (a) Singer, P. T.; Smalas, A.; Carty, R. P.; Mangel, W. F.; Sweet, R. M. *Science* **1993**, *259*, 669−673. (b) Wilmouth, R. C.; Clifton, I. J.; Robinson, C. V.; Roach, P. L.; Aplin, R. T.; Westwood, N. J.; Hajdu, J.; Schofield, C. J. *Nat. Struct. Biol.* **1997**, *4*, 456−462. (c) Wilmouth, R. C.; Edman, K.; Neutze, R.; Wright, P. A.; Clifton, I. J.; Schneider, T. R.; Schofield, C. J.; Hajdu, J. *Nat. Struct. Biol.* **2001**, *8*, 689−694.

(20) Burgi, H. B.; Dunitz, J. D.; Lehn, J. M.; Wipff, G. *Tetrahedron* **1974**, *30*, 1563−1572.

(21) Blow, D. M.; Birktoft, J. J.; Hartley, B. S. *Nature* **1969**, *221*, 337−340.

(22) Corey, D. R.; Craik, C. S. *J. Am. Chem. Soc.* **1992**, *114*, 1784−1790.

(23) (a) Ghosh, D.; Erman, M.; Sawicki, M.; Lala, P.; Weeks, D. R.; Li, N. Y.; Pangborn, W.; Thiel, D. J.; Jornvall, H.; Gutierrez, R.; Eyzaguirre, J. *Acta Crystallogr. D* **1999**, *55*, 779−784. (b) Liao, D. I.; Breddam, K.; Sweet, R. M.; Bullock, T.; Remington, S. J. *Biochemistry* **1992**, *31*, 9796−9812.

(24) (a) Ash, E. L.; Sudmeier, J. L.; Day, R. M.; Vincent, M.; Torchilin, E. V.; Haddad, K. C.; Bradshaw, E. M.; Sanford, D. G.; Bachovchin, W. W. *Proc. Natl. Acad. Sci. U.S.A.* **2000**, *97*, 10371−10376. (b) Day, R. M.; Thalhauser, C. J.; Sudmeier, J. L.; Vincent, M. P.; Torchilin, E. V.; Sanford, D. G.; Bachovchin, C. W.; Bachovchin, W. W. *Protein Sci.* **2003**, *12*, 794−810.

(25) (a) Ishida, T.; Kato, S. *J. Am. Chem. Soc.* **2003**, *125*, 12035−12048. (b) Molina, P. A.; Jensen, J. H. *J. Phys. Chem. B* **2003**, *107*, 6226−6233. (c) Topf, M.; Varnai, P.; Richards, W. G. *J. Am. Chem. Soc.* **2002**, *124*, 14780−14788.

(26) (a) Chakravarty, B.; Gu, Z. W.; Chirala, S. S.; Wakil, S. J.; Quiocho, F. A. *Proc. Natl. Acad. Sci. U.S.A.* **2004**, *101*, 15567−15572. (b) Pazirandeh, M.; Chirala, S. S.; Huang, W. Y.; Wakil, S. J. *J. Biol. Chem.* **1989**, *264*, 18195−18201.

(27) Devedjiev, Y.; Dauter, Z.; Kuznetsov, S. R.; Jones, T. L. Z.; Derewenda, Z. S. *Structure* **2000**, *8*, 1137−1146.

(28) (a) Acevedo, O.; Jorgensen, W. L. *Acc. Chem. Res.* **2010**, *43*, 142−151. (b) Lin, H.; Truhlar, D. G. *Theor. Chem. Acc.* **2007**, *117*, 185−199. (c) Senn, H. M.; Thiel, W. *Angew. Chem., Int. Ed.* **2009**, *48*, 1198−1229.

(29) (a) Kridel, S. J.; Lowther, W. T.; Pemble, C. W. *Expert Opin. Invest. Drugs* **2007**, *16*, 1817−1829. (b) Richardson, R. D.; Ma, G.; Oyola, Y.; Zancanella, M.; Knowles, L. M.; Cieplak, P.; Romo, D.; Smith, J. W. *J. Med. Chem.* **2008**, *51*, 5285−5296.

(30) Drawz, S. M.; Bonomo, R. A. *Clin. Microbiol. Rev.* **2010**, *23*, 160−201.

(31) Maveyraud, L.; Massova, I.; Birck, C.; Miyashita, K.; Samama, J. P.; Mobashery, S. *J. Am. Chem. Soc.* **1996**, *118*, 7435−7440.